Computers and Geotechnics 108 (2019) 75–87

Contents lists available at ScienceDirect

Computers and Geotechnics

journal homepage: www.elsevier.com/locate/compgeo

Research Paper

Seismic behavior and design of strutted diaphragm walls in sand

Mohammad Bahrami, Mohammad Iman Khodakarami*, Abdolhosein Haddad

Faculty of Civil Engineering, Semnan University, Semnan, Iran

ARTICLE INFO

Keywords:
Braced excavation
Diaphragm wall
Seismic design
Steel strut
Significant duration

ABSTRACT

In this paper, the seismic behavior and design of strutted diaphragm wall are evaluated in a dry cohesionless soil. The method of ACI 318 code for designing wall and also Peck's method under AISC regularization for designing steel strut have been discussed. The results indicated that conventional methods of wall and strut design have an acceptable performance in static condition, but when it is subjected to seismic loads, these methods return the values of bending moment and shear force of wall up to 2.8 times and the axial stress in strut up to 11 times larger than allowable limits.

1. Introduction

The increasing city population has led to an increase in transportation system and associated environmental problems are considered to be the main reasons behind the construction of underground structures in urban areas. The use of underground space requires excavation. Since the space for slope excavation is limited in urban areas, cutting is done vertically. Retaining walls are used to prevent large and unsafe soil displacement of the areas around the openings. Diaphragm walls are a kind of retaining walls which are expensive but save time and space and are also safe, so are widely used in underground urban constructions. The horizontal movements of diaphragm walls are usually prevented by horizontal struts. Previously, braced excavation has been investigated by numerical methods in static condition [1–12]. Furthermore, by using empirical and semi-empirical approaches, the behavior of excavations in static mode based on various data from excavations around the world is predicted [13–18]. The present paper is a part of a series of research on braced excavations where seismic behavior and design of diaphragm wall and steel strut were evaluated. It is worth noting that the results of other studies on braced excavation have been previously published by authors, laying out the research background and evolution [12,19].

Madabhushi and Zeng [20] investigated seismic behavior of gravity quay walls numerically and experimentally. They provided new quantitative techniques for absorbing boundaries used in the centrifuge experiments to simulate the free field condition. Caltabiano et al. [21] developed a new solution for the analysis of wall-soil systems based on pseudo-static equilibrium. Gazetas et al. [22] investigated the magnitude and distribution of dynamic earth pressures on L-shaped reinforced-concrete walls, piled walls with horizontal or strongly inclined anchors, and reinforced-soil walls with the help of numerical finite element method. They showed that when the degree of realism in the analysis increases, satisfactory performance of such retaining systems during strong seismic shaking is justifiable. Psarropoulos et al. [23] developed dynamic earth pressure distribution on rigid and flexible walls with the help of the finite element method. Their research indicated that the results of Mononobe–Okabe and elasticity-based solutions for structurally or rotationally flexible walls are close. Wartman et al. [24] analyzed the seismic behavior of earthquake by studying four mechanically stabilized earth (MSE) walls under Tecoman, Mexico. They discussed the applicability and validity of the pseudo-static and sliding block methods of seismic analyses based on observed performance. Callisto and Soccodato [25] studied seismic behavior of cantilever retaining wall under two Italian earthquakes in dry coarse-grained soil with numerical and pseudo-static approach in order to provide guidance for design. They utilized plane-strain finite-difference numerical analyses. Eventually, they developed an economic criterion to design these underground structures that relies on the ductility of the system. Chowdhury et al. [26] examined seismic behavior of diaphragm wall under the three earthquakes with different peak ground accelerations (PGAs) using finite difference numerical methods. They recommended penetration depth and thickness of the diaphragm walls for 10–20 m excavation equal to 100 and 6% of the final depth of the excavation under seismic loads. Konai et al. [27] investigated the seismic behavior of braced excavation in dry sand with experimental and numerical approaches. Their study revealed that increase of excavation depth and the amplitude of base acceleration lead to increased lateral displacement, bending moment, strut forces and maximum ground surface displacement.

Diaphragm walls are made in many parts of the world. Since these underground structures are mainly constructed in earthquake-prone

* Corresponding author.
E-mail address: khodakarami@semnan.ac.ir (M.I. Khodakarami).

https://doi.org/10.1016/j.compgeo.2018.12.019
Received 31 July 2018; Received in revised form 17 November 2018; Accepted 18 December 2018

Nomenclature

α	non-dimensional frequency factor
γ	soil unit weight
λ	wavelength
μ	poisson's ratio
ρ	density
ϕ	friction angle of soil
ϕ_m	strength reduction factor for bending moment
ϕ_v	strength reduction factor for shear
σ	mean stress of soil
ω_n	natural frequencies of site
ω_e	frequency of earthquake
Δl	element size
Δz_{min}	smallest width of the interface adjacent mesh
a_i	loading height for strut
b	width of the unit
E_s	Young's modulus of soil
E_0	Young's modulus at reference pressure
f	frequency
f_a	maximum existing stress of strut
F_a	allowable stress
F_i	force of each strut
F_{se}	seismic force of strut
F_{st}	static force of strut
G	shear modulus
G_0	small strain shear modulus
G_{st}	shear modulus in static condition
H_e	final excavation depth
H_g	thickness of the soil layer
K_0	coefficient of lateral earth pressure at rest
K_a	Rankine's coefficient of earth pressure
K_d	bulk modulus in dynamic condition
K_{st}	bulk modulus in static condition
K_n	normal stiffness
K_s	shear stiffness
L_F	load resistance factor
M	bending moment obtained from analysis
M_n	nominal bending moment
M_u	bending moment for design
N	average value of standard penetration test
P	soil pressure
P_{ref}	reference pressure
s	horizontal distance of bracing
T_p	predominant period
V	shear obtained from analysis
V_n	nominal shear
V_s	shear wave velocity
V_u	ultimate shear force for design
z	depth

regions, it is important to understand their seismic behavior in order to design these structures to be resilient against earthquake loading. The earthquake forces may result in collapse of diaphragm wall or failure of struts. Since only limited research has been done on seismic behavior and design of diaphragm walls and lateral braces, in this study, the behavior of these walls and lateral steel struts has been evaluated under Tabas, Whittier Narrows and Northridge earthquakes using finite difference numerical method. Analysis has been done in two types of sand with different stiffness. Excavation depth was considered as 10 m and two rows of struts were installed to reduce wall deflection. Acceleration time history of significant duration of the earthquakes has been applied into the bedrock with depths of 30, 60 and 90 m as seismic input. In the present paper, in addition to the verification and sensitivity analysis, a total of 18 cases were modeled and analyzed, and the results in terms of bending moment and shear forces of wall and also stress of struts were evaluated and interpreted in detail.

2. Numerical simulation

All static and seismic analyses of this study were performed using the two-dimensional plane strain finite difference software FLAC2D [28]. Both the width and depth of excavation are considered to be 10 m. Excavation procedure has been modeled with three-step cutting and two-step bracing. Struts arrangement was selected according to the design guide of Chowdhury et al. [10] and also thickness and penetration depth of diaphragm wall were selected to be 60 cm and 10 m, as recommended by Chowdhury et al. [26]. The wall properties such as Young's modulus, density and Poisson's ratio were equal to 29580 MPa, 2100 kg/m^3 and 0.15, respectively. The geometry, boundary condition and symbols used in analysis are presented in Fig. 1. In this figure, H_e is the final excavation depth and H_g measures the distance between ground surface and bedrock.

Two types of loose sand ($N < 10$) and dense sand ($30 < N$) were studied, while N is the average value of standard penetration test. The

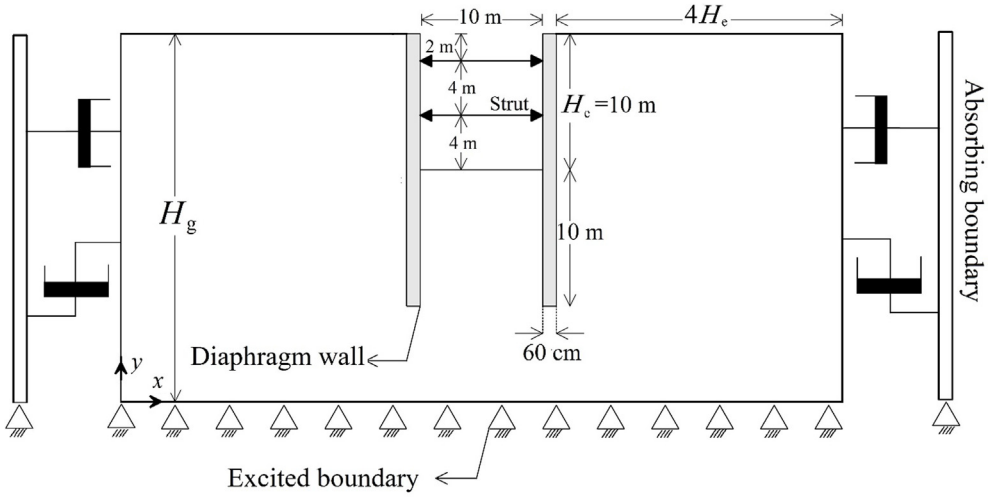

Fig. 1. The cross-section of model.

properties of these two types of sandy soil have been taken from O6 station on the orange line in the Kaohsiung rapid transport system (KRTS), which has been previously reported in Hsiung research [8]. The stiffness of the surface soil layer is obtained from Ohsaki, and Iwasaki [29] equation. In this equation, small strain shear modulus in MPa is given by:

$$G_0 = 6.374N^{0.94} \tag{1}$$

The soil stiffness is assumed to increase with depth according to the Janbu [30] relation:

$$E_s(z) = E_0\left(\frac{\sigma(z)}{P_{ref}}\right) \tag{2}$$

where, E_s denotes Young's modulus of soil and σ is the mean stress due to the soil self-weight which is determined as follows:

$$\sigma(z) = \begin{cases} \frac{(1+2K_0)\gamma z}{3} & z \geq z_0 \\ \sigma(z_0) & z < z_0 \end{cases} \tag{3}$$

where, z denotes depth, γ is soil unit weight, P_{ref} is a reference pressure (100 kPa), E_0 designates the Young's modulus when $\sigma = P_{ref}$ and z_0 is the thickness of the surface soil layer, which is assumed to have a constant stiffness. K_0 is the coefficient of lateral earth pressure at rest, which is calculated from Jaky [31] equation $(1 - \sin\phi)$. The relationship between the Young's modulus (E) and the shear modulus (G) of the soil is expressed by:

$$E = 2G(1 + \mu) \tag{4}$$

where, μ is Poisson's ratio.

To incorporate the soil stiffness in numerical analysis, a reduced coefficient has been used during static analyses as proposed by Aversa et al. [32]. Each simulation procedure was performed with two soil properties, soil in static condition analyses with 0.3 G_0 and under seismic situation analyses with G_0. First, the wall has been built in the soil with the seismic properties. Then, soil properties are changed in static condition and the excavation and bracing are done up to the final depth of the excavation. At the end of the excavation, soil properties have been changed in seismic mode again, and seismic loads are applied to the model. This procedure was performed because in static condition, the model does not allow change in soil stiffness with the strain level. The bulk modulus of the soil in static (K_{st}) and dynamic (K_d) analysis was obtained by the following equations:

$$K_{st} = \frac{2(0.3G_0)(1+\mu)}{3(1-2\mu)} \tag{5}$$

$$K_d = \frac{2(G_0)(1+\mu)}{3(1-2\mu)} \tag{6}$$

The properties of two type of sand are presented in Table 1. In this table, μ is Poisson's ratio, ρ is density and ϕ is the friction angle of soil. In Table 1, G_{st} is shear modulus of soil in static analyses and is equal to 0.3 G_0.

Soil and wall interaction has been modelled by the interface parameters including friction angle, normal stiffness and shear stiffness. The normal and shear stiffness are simulated by using springs which are connected to each node of the wall. The normal and shear springs model the lateral motion and the vertical displacement between the wall and the surrounding soil, respectively. In all numerical simulations, the interface friction angle was considered to be equal to $2/3\phi$. In addition, the normal stiffness (K_n) and the shear stiffness (K_s) are also calculated by the following relation:

$$K_n = K_s = 10\max\left[\frac{K_d + \frac{4}{3}G_0}{\Delta z_{min}}\right] \tag{7}$$

where, Δz_{min} is the smallest width of the interface adjacent mesh in the normal direction. The normal and shear stiffness (K_n and K_s) considered for the numerical study was 1286 MPa/m for loose sand and 4370 MPa/m for dense sand.

The design of a diaphragm wall includes the design of wall thickness and reinforcements. Thickness of a diaphragm wall in preliminary design is generally set to about 4–8% of the excavation depth. In the present research, following Chowdhury et al. [26], the wall thickness was considered as 6% of the excavation depth and also reinforcement design and nominal strength calculation were performed using the so-called strength design method or LRFD methodology based on ACI 318–14 code [33]. Diaphragm wall design is undertaken based on bending moment and shear envelope obtained from the stress analysis. In the design of such underground walls, width of the unit (b) is considered as one meter, and the wall is analyzed under plane strain condition. Since the length-to-width ratio of excavations is generally large, plane strain conditions can be assumed. In ACI 318 code, the designed and nominal bending moment and shear are calculated via the following relationships:

$$M_u = L_F M \tag{8}$$

$$M_n = \frac{M_u}{\phi_m} \tag{9}$$

$$V_u = L_F V \tag{10}$$

$$V_n = \frac{V_u}{\phi_v} \tag{11}$$

in which,

M: bending moment obtained from analysis
M_u: bending moment for design
M_n: nominal bending moment
V: shear obtained from analysis
V_u: shear for design
V_n: nominal shear
L_F: load resistance factor; according to ACI (2014), L_F is equal to 1.6
ϕ_m: strength reduction factor for bending moment; according to ACI (2014), ϕ_m is equal to 0.9
ϕ_v: strength reduction factor for shear; according to ACI (2014), ϕ_v is equal to 0.75

In this study, compressive strength of concrete, yield strength of reinforcements, and reinforcement ratio were set to 30 MPa, 400 MPa, and 0.02, respectively. Finally, based on the present analysis, nominal bending moment and nominal shear force were calculated as 2039 kN.m and 934 kN, respectively.

Because lateral supports are generally designed under static loads, these supports may fail under seismic conditions. In the present paper, the effect of seismic loads on the stability of struts designed using traditional method has been discussed. Struts are made from steel with density of 7850 kg/m^3 and Young's modulus of 2×10^8 kN/m^2. They are designed based on the theory of beam-column under the AISC code [34]. In order to design struts, Peck's method [35] was employed for determining the soil pressure and the load distance of each strut. In this

Table 1
The properties of soil in numerical modeling (Data from Hsiung [8]).

Soil type	SPT-N values	G_0 (*MPa*)	K_d (*MPa*)	G_{st} (*MPa*)	K_{st} (*MPa*)	μ	ϕ (Degree)	ρ (*kg/m^3*)
Loose sand (LS)	5–14	53	58	15.9	17.4	0.3	32	2008
Dense sand (DS)	28–42	180	197	54	59.1	0.3	33	2028

method, sandy soil pressure is equal to:

$$P = 0.65_{\gamma} H_e K_a \quad (12)$$

where, γ is soil unit weight and K_a is Rankine's coefficient of earth pressure ($\tan^2(45 - \phi/2)$). Fig. 2 presents the pressure exerted on the walls and load height for each strut. In this figure, F_i is the force applied on each strut, a_i denotes loading height for any strut and s is horizontal distance of bracing. The results of struts design are provided in Table 2. Details of construction and simulation of excavation procedures are presented step by step in Table 3.

Earthquake may occur at any stage of the construction process of excavation. However, the maximum chance of earthquake occurrence is at the end of construction. Therefore, in this study, acceleration time histories of earthquakes were applied to the bedrock at the end of construction. The soil layer was underlain by rigid layer at the bottom of the model. In the wall construction, excavation and bracing procedures (in static analyses), the lateral model boundaries were restrained from movement in horizontal direction (which is fixed along x direction) and the lowest depth of the model was restrained from moving in both horizontal and vertical directions (which is fixed along x and y directions). During seismic analyses, free-field boundaries were applied along the vertical boundaries of the model. Free-field boundaries retained their non-reflecting properties under dynamic simulation. The main grids of the lateral boundaries were joined with the free-field by viscous dashpots to simulate quiet boundary condition as developed by Lysmer and Kuhlemeyer [36]. The status of boundary conditions in seismic analysis is shown in Fig. 1.

Despite the widespread usage by engineers for retaining wall design, the pseudo-static method has some restrictions. In this study, the time history method which is able to achieve more precise results for the seismic analysis of underground structures is used due to the limitations of the pseudo-static method. In order to evaluate the seismic behavior of wall, acceleration time histories of three earthquakes of Tabas, Whittier Narrows and Northridge after the last stage of excavation, were applied on the bedrock. Table 4 presents the details of chosen the earthquakes. In this table, T_p is predominant period of earthquakes. Tabas and Whittier Narrows earthquakes although possessing close peak ground acceleration (PGA) and duration, were quite different in terms of significant duration. Northridge earthquake has a high PGA and its significant duration is between the two other earthquakes. Therefore, the effect of PGA and significant duration of earthquake on the braced wall behavior by applying these acceleration time histories as seismic input have been assessed. Indeed, the main purpose of this paper is to determine the safety of the usual diaphragm walls under seismic loads. The PGA values of the chosen earthquakes are high enough and the range of significant duration is wide enough to cover most of the earthquakes that occurred. Figs. 3–5 present the acceleration time history of Tabas, Whittier Narrows and Northridge earthquakes, respectively.

Table 2
The properties of the struts used in the numerical analysis.

Section provided	Cross-section area ($m^2 \times 10^{-4}$)	Second moment area ($m^2 \times 10^{-8}$)
H390 × 300 × 10 × 16	133.3	37,900

Table 3
The simulation procedures.

Steps	Simulation details
Step 1	Initial equilibrium in the seismic soil properties.
Step 2	Construction of diaphragm wall in seismic soil properties.
Step 3	Reduced coefficient applied to the soil properties.
Step 4	Considering all displacements equal to zero and excavation up to a depth of 3 *m*.
Step 5	Installation of strut at depth of 2 *m*.
Step 6	Excavation up to a depth of 7 *m*.
Step 7	Installation of strut at a depth of 6 *m*.
Step 8	Excavation up to a depth of 10 *m*.
Step 9	Seismic soil properties applied to the model again.
Step 10	Applying dynamic boundaries and soil damping.
Step 11	Acceleration time history applied to the bedrock.

In the analyses of this paper, development of irreversible deformations causes complete energy dissipation. The seismic soil behavior is defined by non-linear model and each step of computation of shear modulus was updated using hysteretic model and also followed elastic-perfectly plastic soil model with a Mohr-Coulomb failure criterion. The slight Rayleigh viscous damping was considered to be equal to 1% for the soil considering negligible variations in the calculated movements and internal forces in the embedded diaphragm wall.

Significant duration of the strong ground motion was defined as the time interval between the 5% and the 95% of the Arias intensity by Trifunac and Brady [37]. Since seismic studies are very time consuming, using significant duration of earthquake for seismic analysis can save time. Fig. 6 illustrates the curves of the Arias intensity versus time for all three earthquakes. In this figure, Arias intensity of 5 and 95% is depicted by two horizontal dash lines and the duration of Arias

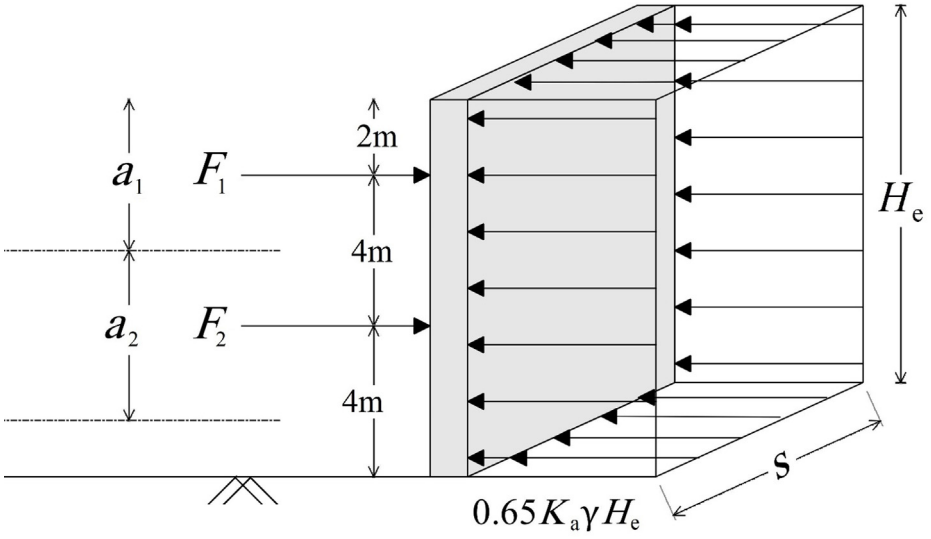

Fig. 2. The apparent earth pressure diagram and load distance of struts.

Table 4
Details of considered earthquakes.

Earthquake name	Year	PGA (*g*)	Duration (sec.)	Significant duration (sec.)	T_p (sec.)
Tabas	1978	0.32	21	11.32	0.20
Whittier Narrows	1987	0.36	21	1.22	0.14
Northridge	1994	0.73	25	5.87	0.38

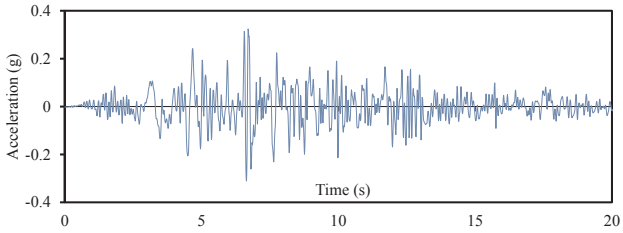

Fig. 3. Acceleration time history of Tabas earthquake.

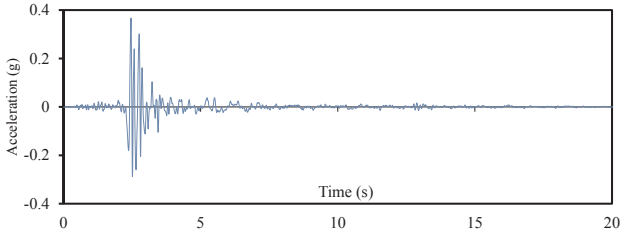

Fig. 4. Acceleration time history of Whittier Narrows earthquake.

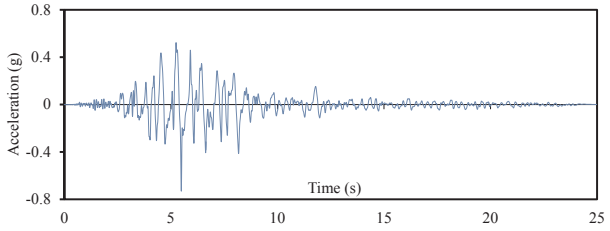

Fig. 5. Acceleration time history of Northridge earthquake.

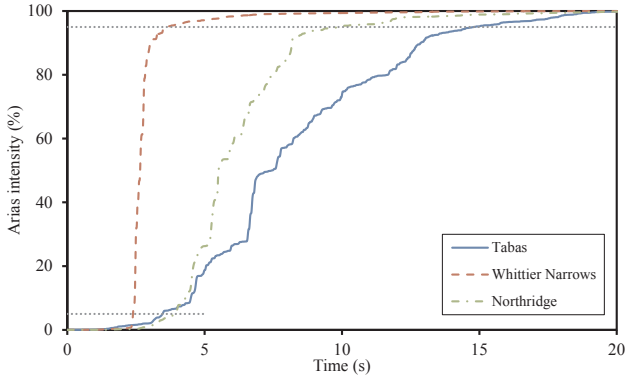

Fig. 6. The Arias intensity vs. time.

intensity variation between these quantities is comparable. As shown in the graphs presented in Fig. 6, Tabas earthquake applies its energy for a longer duration to the site than the two other earthquakes.

For a vertically propagating waves through a homogeneous soil, the natural frequencies of vibration are given by following the equation provided by Kramer [38]:

$$\omega_n = V_s(2n-1)/4H_g \quad n = 1, 2, 3\cdots \tag{13}$$

where, ω_n is the n^{th} natural frequency of the vibrating soil medium. By increasing the depth of bedrock, the natural frequency of the site is reduced. The frequency of earthquake is defined by:

$$\omega_e = 2\pi/T_p \tag{14}$$

And the non-dimensional frequency factor is defined as:

$$\alpha = \omega_e/\omega_1 \tag{15}$$

where, ω_1 is the first natural frequency of site.

Therefore, the two types of soils have been assessed and the seismic input is applied to the bedrock at depths of 30, 60 and 90 m to evaluate the seismic behavior and design of braced excavation in wide range of α parameters.

In the numerical analysis, wave propagation conditions must be prepared in the finite difference mesh configuration. Two factors of the input, wave frequency and wave speed are effective for numerical precision of wave propagation in the model. Kuhlemeyer and Lysmer [36] demonstrated that for propagation of wave in a continuum, the element size (Δl) should be approximately one-tenth of the wavelength of the highest frequency component of incoming wave; such as:

$$\Delta l = \lambda/10 \tag{16}$$

in which, wavelength and frequency are related to each other using the shear wave velocity (V_s); which is calculated by,

$$V_s = \sqrt{\frac{G_0}{\rho}} \tag{17}$$

The relationship between frequency and wavelength is as follows:

$$f_{Max} = V_s/\lambda \tag{18}$$

Therefore, by filtering the acceleration time history with a desirable maximum frequency, the conditions of wave propagation in the meshing configuration can be provided. In this research, since the least shear modulus in seismic analysis is 53 MPa, the shear wave velocity obtained is 162 m/s. Dimensions of all meshes in this study are considered to be equal to 1 m × 1 m. Due to the above, maximum frequency which can be applied on the model is 16.2 Hz. So, the input of acceleration time histories has been filtered with frequency of 15 Hz. It should be noted that sensitivity analysis was performed on mesh size and model geometry for the studied frequency contents, based on which results boundary distance and mesh configuration were determined.

Filtering of the acceleration time histories has led to the loss of a part of the earthquakes energy. Therefore, it is important to study the power of seismic energy remains after filtering earthquake acceleration time history. Figs. 7–9 present Fourier amplitude spectrum of Tabas, Whittier Narrows and Northridge earthquakes, respectively. For all

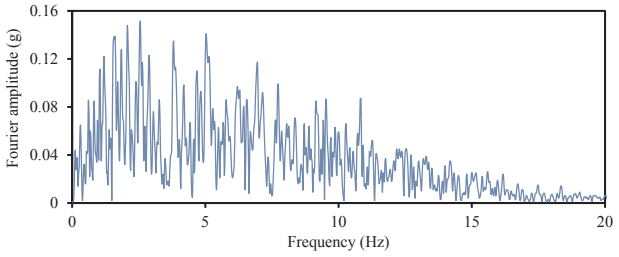

Fig. 7. Fourier amplitude spectrum of Tabas earthquake.

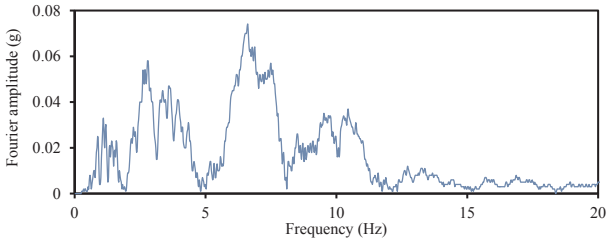

Fig. 8. Fourier amplitude spectrum of Whittier Narrows earthquake.

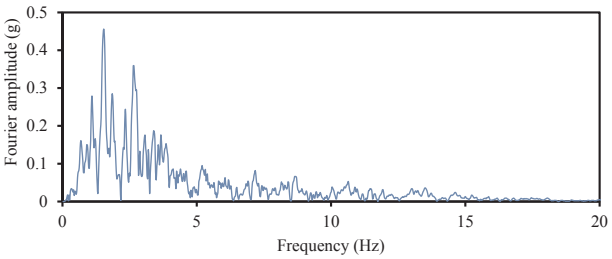

Fig. 9. Fourier amplitude spectrum of Northridge earthquake.

three earthquakes, the majority of the earthquake power is contained within the 15 Hz frequency. Fig. 10 presents cumulative Fourier amplitude curves of all three earthquakes. Filtering acceleration time histories of Tabas, Whittier Narrows and Northridge earthquakes with a frequency of 15 Hz will lead to loss of only 6, 12 and 3% of their energy as shown in cumulative Fourier amplitude curves. Therefore, even after filtering, the natural seismic motion remained.

3. Verification

In order to validate the modeling procedure, seismic behavior of a diaphragm wall is modeled as presented by Chowdhury et al. [26] after the Friuli earthquake. Fig. 11 presents the acceleration time history of Friuli earthquake. Both the width and depth of the excavation are 10 m and penetration depth of wall is 8 m. The horizontal boundary of bottom extends up to 60 m below the toe of the wall.

First, a diaphragm wall with elasticity modulus (E_{wall}), Poisson ratio (μ_{wall}), and wall thickness of respectively 29,580 GPa, 0.15, and 60 cm was constructed on a soil with seismic properties. Then by applying the soil static properties to the model, excavation and bracing were performed to a depth of 10 m. Two struts are installed at depth of 2 and 6 m. Finally, by assigning seismic properties of the soil and assigning dynamic boundary conditions, the acceleration time history of earthquake was applied to the bedrock. Rayleigh damping was considered to be equal to 1% for the soil. All the material properties are taken as reported in Chowdhury et al. [26]. The sandy soil properties for verification are presented in Table 5.

The comparison between the results of wall bending moment in the present paper and those from Chowdhury et al. [26] is presented in Fig. 12. The dynamic diagrams of Fig. 12 correspond to the end of earthquake. The consistency of the present research results with the results of the analysis conducted by Chowdhury et al. [26] indicates the validity of the current modeling procedure. In the present paper, the significant duration of the Friuli earthquake is applied to the model, while the entire duration of the earthquake has been applied by Chowdhury et al. [26]. The similarity of the results of the current research with the results provided by Chowdhury et al. [26] shows that the significant duration of the earthquake will produce results similar to applying the entire earthquake time to the model. The little difference between the current research results and Chowdhury et al. [26] is due to the differences of time-step in dynamic analyses, different meshing configurations and the duration of seismic inputs.

4. Analysis results and discussion

The effects of Tabas, Whittier Narrows and Northridge earthquakes on the behavior and design of strutted wall have been discussed in this section. The bending moment and shear forces of wall and also the forces exerted to the lateral supports are investigated and the results of numerical simulation have been presented in details.

4.1. Seismic behavior of diaphragm wall

In Figs. 13 and 14, flexural and shear behaviors of the wall in the static state are illustrated for the last stage of excavation, respectively. As can be observed in these two figures, the process and pattern of the wall behavior throughout its depth are almost the same for both soil types except that the analysis results in the wall depth, except to the depth of 2 m, contain more amounts in the loose sand compared to the dense sand.

A total of 21 points were considered at a distance of one meter along the depth of each wall, and the behavior of these points was observed during the seismic loading. The maximum and minimum of bending moment and shear force of diaphragm wall at each point in positive and negative range were recorded. By drawing a diagram with these maximum and minimum values at any point, two positive and negative envelope diagrams are prepared for each wall. As an example, in Figs. 15 and 16, flexural and shear behaviors of two separate elements of the modeled diaphragm wall during the entire time of dynamic analysis are presented. The element which shows its flexural behavior in Fig. 15 is located in a depth of 8 m from the ground level on the right wall, and has been analyzed in loose sand under Tabas earthquake. Moreover, the element which presents its shear behavior in Fig. 16 is located into a depth of 18 m from the ground level on the left wall, and has been evaluated in dense sand under Northridge earthquake. In both cases, the seismic load is considered to be applied to bedrock located into a depth of 30 m.

Considering the flexural behavior of the element shown in Fig. 15, the maximum positive bending moment of the element was recorded at the 18,280th dynamic cycle. Furthermore, given that negative bending moment was not observed at any point, zero minimum flexural moment was recorded at this point. During the course of an earthquake, the range of variations of the flexural momentum of the element exhibited very large fluctuations. However, once the loading to the bedrock was terminated at say 124,000th step, the range of variations was seen to become narrow. In addition, based on the shear behavior of the element presented in Fig. 16, a maximum shear of about 483 kN was recorded for this element of the wall at the 54,860th dynamic cycle. Moreover, minimum shear (−91 kN) was observed at the 4910th cycle. As it is evident in Fig. 16, upon termination of load application to the bedrock, the range of variations of shear force also became limited.

Figs. 17–22 present the bending moment and shear forces envelopes

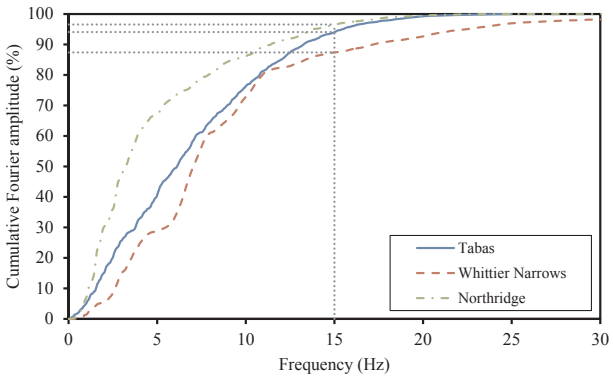

Fig. 10. Cumulative Fourier amplitude spectrum of earthquakes.

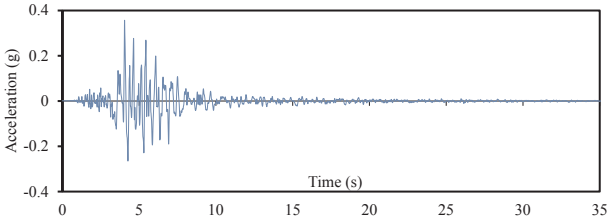

Fig. 11. Acceleration time history of Friuli earthquake.

Table 5
The properties of soil in verification analysis.

G_0 (*MPa*)	K_d (*MPa*)	G_{st} (*MPa*)	K_{st} (*MPa*)	μ	ϕ (Degree)	Density (kg/m^3)
210	455	63	136.5	0.3	35	2040

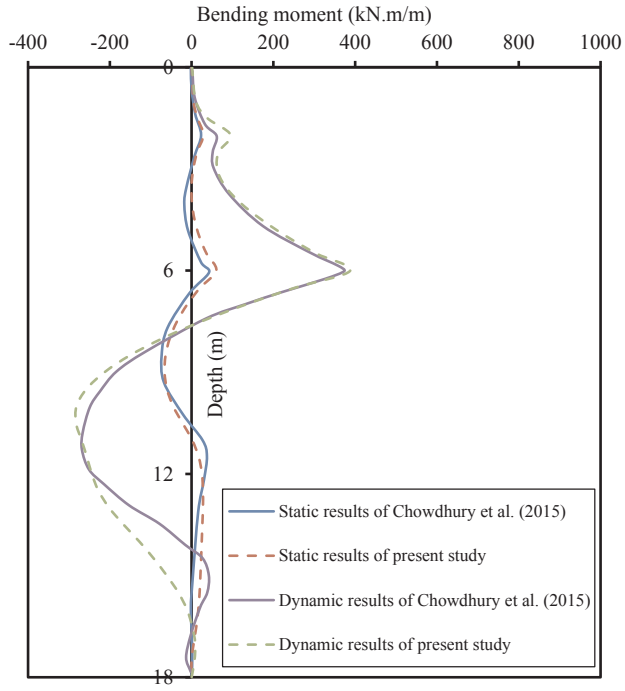

Fig. 12. The comparison between the wall bending moment in the present study and in the study of Chowdhury et al. [26].

of left wall in the loose sand under seismic loading. In these figures, the effect of bedrock depth on the wall behavior has been evaluated by applying acceleration time history to bedrocks with depths of 30, 60 and 90 m. It could be concluded from the above-mentioned diagrams that the pattern behavior of wall is similar under all three bedrock depths for each seismic loading and in general, increase in the bedrock depth causes reduction of bending moment and shear forces in the diaphragm wall. As shown in these figures, in braced depths (i.e. 2 and 6 m), sudden change in wall behavior has been observed. By increasing the bedrock depth from 30 to 60 m, the maximum wall bending moment is reduced to about 24% under Tabas and Whittier Narrows earthquakes and about 27% under Northridge earthquake and also the maximum wall shear force is reduced by about 19 and 21% under Tabas and Northridge earthquakes, respectively. However, the increase of bedrock depth from 60 to 90 m has a lesser effect on the wall bending moment and shear force reduction. By increasing the bedrock depth from 60 to 90 m, the bending moment and the shear forces of the wall are reduced to about 8 and 11%, respectively under Tabas earthquake and also, these two outputs are reduced to about 23% under Northridge earthquake. Furthermore, the changing of bedrock depth has a

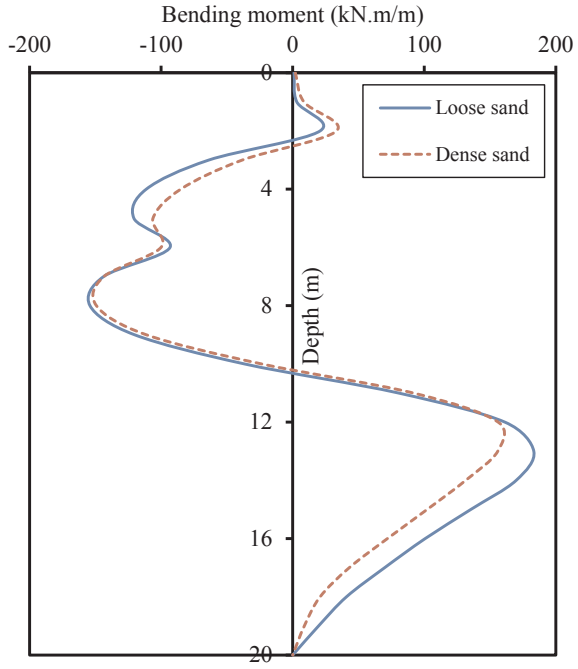

Fig. 13. The static flexural behavior of the wall after last excavation.

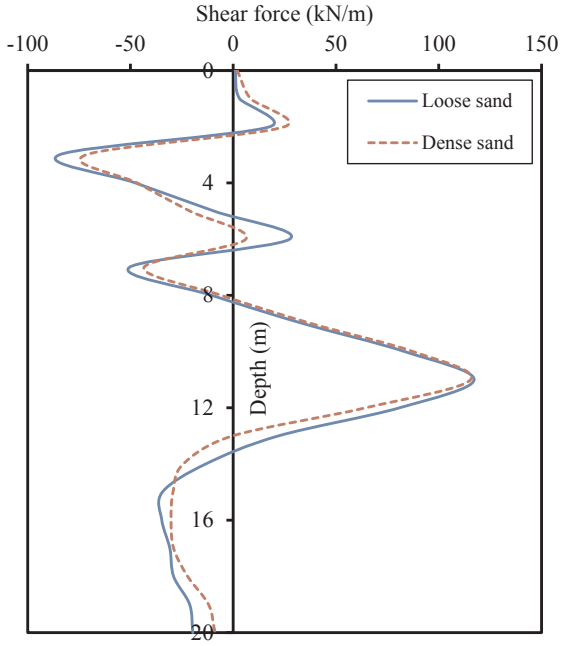

Fig. 14. The static shear behavior of the wall after last excavation.

negligible effect on maximum wall shear force under Whittier Narrows earthquake. Considering the wall behavior shown in Figs. 17–22, it is indicated that variation of bedrock depth has more considerable effects on the wall behavior under high magnitudes of moment and shear. For example, the effects of variation of bedrock depth on the wall behavior under Northridge earthquake are larger than those under Whittier Narrows earthquake since Northridge earthquake leads to intensively higher moment and shear in the wall.

Figs. 23 and 24 present the effect of soil stiffness on seismic behavior of wall when the Northridge earthquake was applied to bedrock located at a depth of 30 m. The wall behavior analysis was performed in two types of sand with different shear modulus. As it can be observed in Fig. 23, bending moment of the wall in loose soil is generally larger

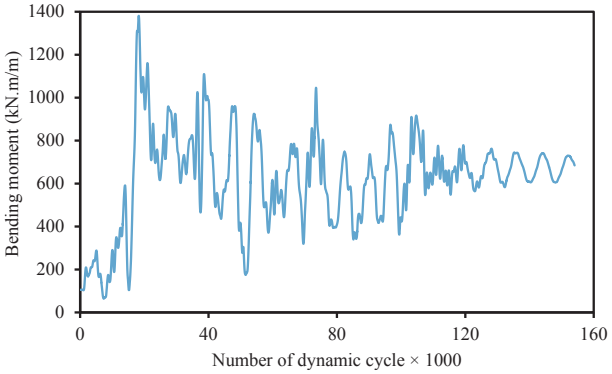

Fig. 15. Flexural behavior of a wall element in the course of seismic loading.

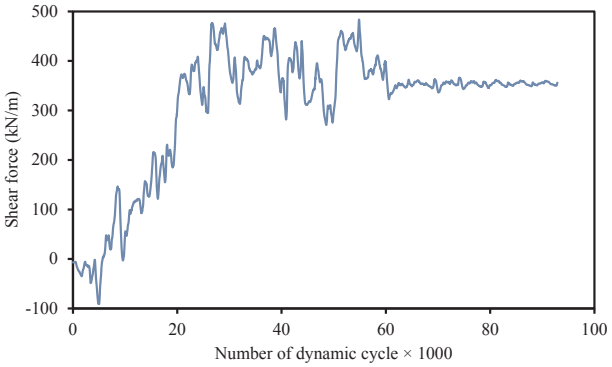

Fig. 16. Shear behavior of a wall element in the course of seismic loading.

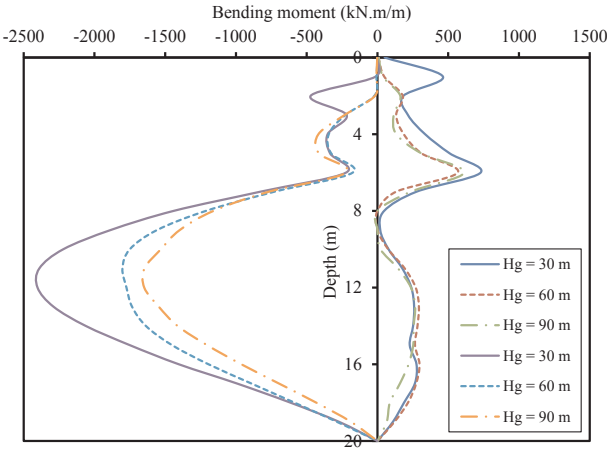

Fig. 17. The effect of bedrock depth on flexural wall behavior under Tabas earthquake.

than dense soil. It is also inferred that by comparing the diagrams presented in this figure, the maximum bending moment of the wall is 21% higher in loose soil compared to dense soil. In accordance to Fig. 24, though shear force values along the wall depth are higher in loose sand but shear force in braced points of the wall has a remarkable jump in dense sand compared to loose sand. Such that for depth of 6 m where the second strut is installed, the shear force of the wall in the dense soil is 54% higher than the loose soil. Hence, the reciprocal bracing method is not a desirable construction method in sites with dense sand in high seismic zones. It should be noted that such pattern of flexural and shear behaviors of walls in the two types of soil is also observed under other earthquakes and bedrock depths.

Fig. 25 presents the comparison of the flexural behaviors of the left and right walls under Tabas earthquake and also Fig. 26 displays the

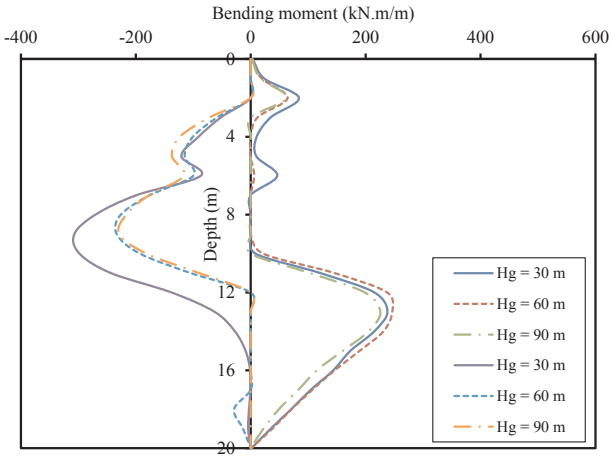

Fig. 18. The effect of bedrock depth on flexural wall behavior under Whittier Narrows earthquake.

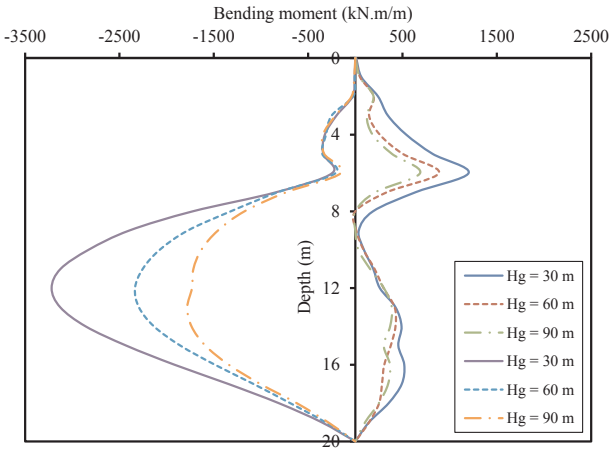

Fig. 19. The effect of bedrock depth on flexural wall behavior under Northridge earthquake.

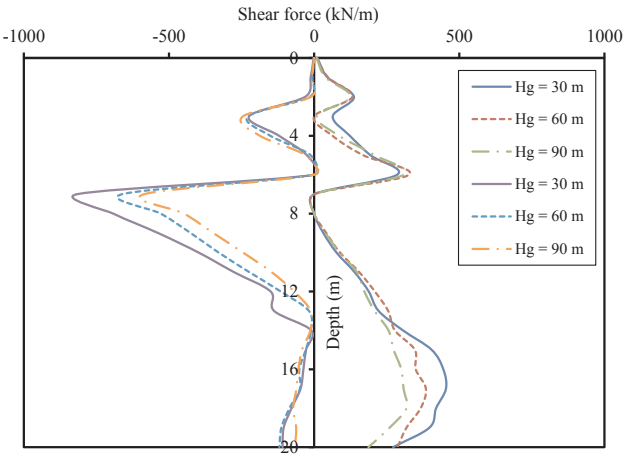

Fig. 20. The effect of bedrock depth on shear wall behavior under Tabas earthquake.

comparison of the shear behaviors of opposite walls under Northridge earthquake in a loose sand with bedrock depth of 30 m. As evident from these two figures, the positive outputs of the right-side wall are symmetrical to the negative values related to the left-side wall. On the contrary, the negative values bending moment or shear force of the right-side wall are almost symmetrical to the positive bending moment

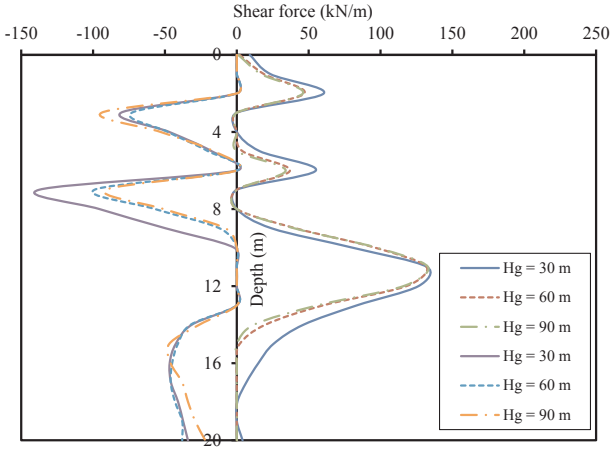

Fig. 21. The effect of bedrock depth on shear wall behavior under Whittier Narrows earthquake.

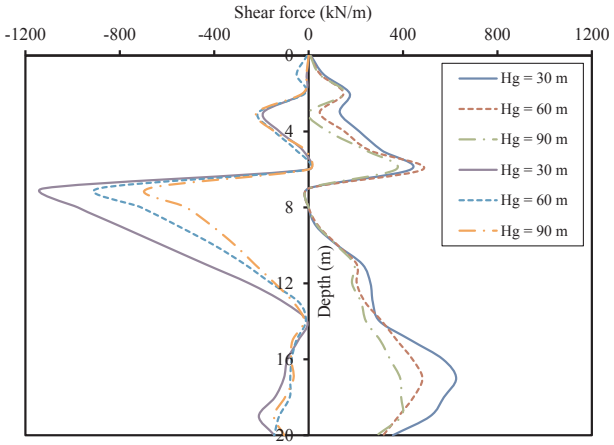

Fig. 22. The effect of bedrock depth on shear wall behavior under Northridge earthquake.

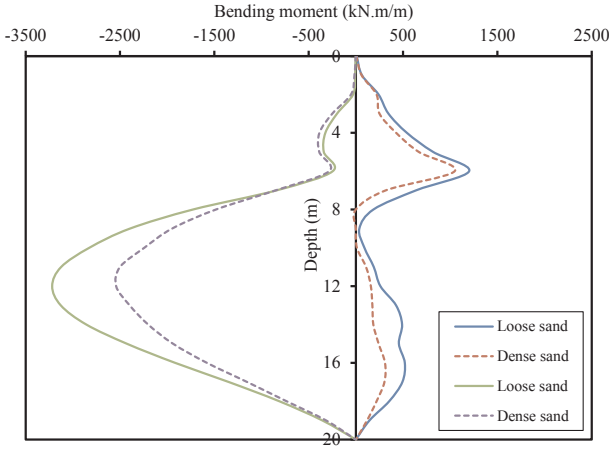

Fig. 23. The effect of soil type on the flexural wall behavior.

or shear force related to the left-side wall. Although opposite walls behavior is slightly different, assessment results variation along the wall depth is the same for the right-side and the left-side walls. This behavioral pattern along the wall depth is repeated at all depths of the bedrocks in both soil types and under every three seismic loading. Therefore, results of a wall are extensible to the opposite one. It is worth noting that the maximum behavioral difference between the opposite

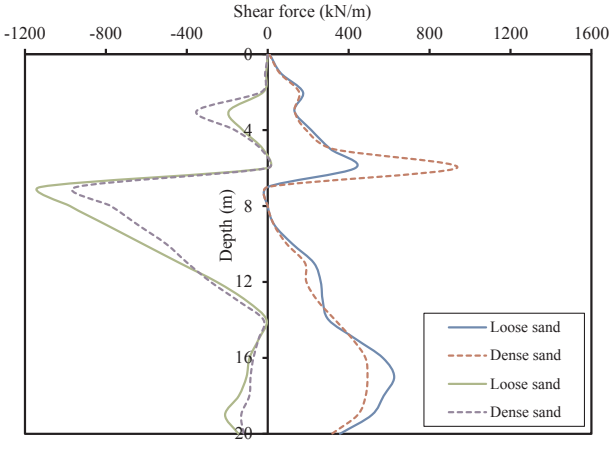

Fig. 24. The effect of soil type on the shear wall behavior.

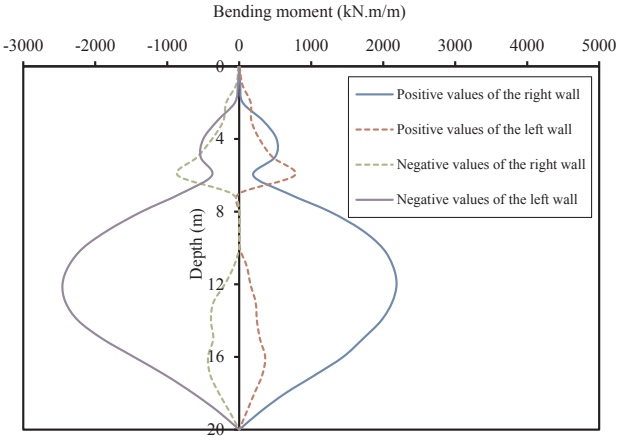

Fig. 25. The Comparison of flexural behavior of right and left walls.

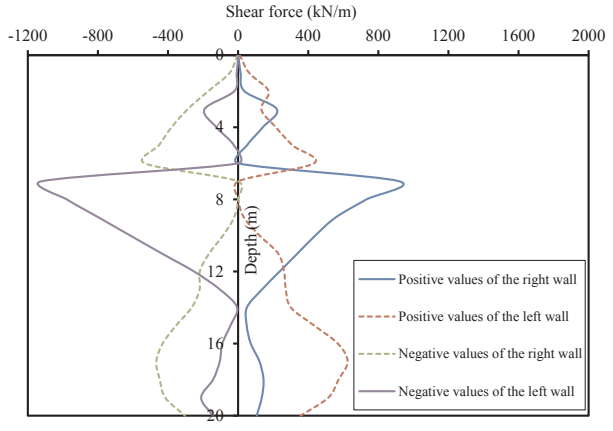

Fig. 26. The Comparison of shear behavior of right and left walls.

walls in the current research is always seen to be less than 20%.

Fig. 27 presents the comparison of bending moment envelope diagrams under every three earthquakes in loose sand when seismic loads were applied to bedrock depths at 30 m. According to the diagrams presented in Fig. 27, it could be seen that the maximum wall moment created by the Northridge earthquake is 25% larger than Tabas earthquake. Furthermore, the maximum wall moment of Northridge and Tabas earthquakes is almost 11 and 8 times larger than Whittier Narrows earthquake outputs. In all depths along the wall, except for areas close to the crest wall, whether positive or negative values, moment

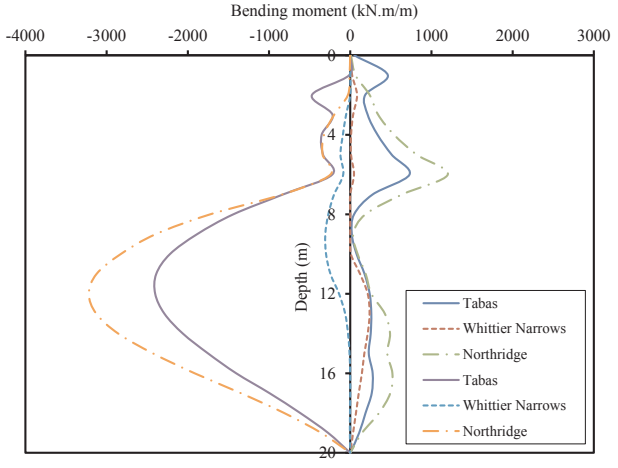

Fig. 27. The comparison of flexural wall behavior under various earthquakes.

envelope diagrams of Northridge earthquake show greater values than the two other earthquakes.

The shear force envelope diagrams under every three earthquakes in loose sand when seismic loads were applied to bedrock depths at 30 m are compared in Fig. 28. According to the diagrams presented in this figure, it could be seen that the maximum shear force of the wall created by the Northridge earthquake is 27% larger than Tabas earthquake. Moreover, the maximum shear force of the wall under Northridge and Tabas earthquakes is almost 8 and 6 times larger than the results of Whittier Narrows earthquake. In all depths along the wall, whether positive or negative values, moment envelope diagrams of Northridge earthquake show greater shear force values than the two other earthquakes.

Summarizing Figs. 27 and 29, it can be concluded that although the PGA of Whittier Narrows earthquake is a little higher than Tabas earthquake, the longer significant duration of Tabas earthquake caused more damaging effects on the diaphragm wall. In addition, it can be observed that Northridge earthquake has high destructive effects on the underground wall regarding its high PGA. Hence, in spite of the considerable effect of earthquake PGA on the performance of underground structures, significant duration of the earthquake is an absolutely important parameter in the analysis of underground walls and its increase has wide destructive impacts on the behavior of these walls. For this reason, the significant duration of an earthquake is considered to be important in the analysis and design of the diaphragm walls.

4.2. Seismic design of diaphragm wall

In this part of the present paper, the efficiency of the current conventional methodology for designing diaphragm wall under seismic loads is evaluated. As explained earlier, the diaphragm walls modeled in this research were designed following the ACI 318 code procedure. According to this method, the design moment/shear should always be lower than the nominal moment/shear considering strength reduction coefficients. In other words, the following two relationships should always be satisfied:

$$M_u \le \phi_m M_n \Rightarrow \frac{M}{M_n} \le \frac{\phi_m}{L_F} = \frac{0.9}{1.6} = 0.56 \quad (19)$$

$$V_u \le \phi_v V_n \Rightarrow \frac{V}{V_n} \le \frac{\phi_v}{L_F} = \frac{0.75}{1.6} = 0.47 \quad (20)$$

where, the M/M_n and V/V_n ratios higher than 0.56 and 0.47, respectively, indicated incompliance of the results of the numerical analysis with the requirements set in ACI 318. That is, in case the above-mentioned conditions come true, the safety of the underground wall will be at risk.

In case of static analysis, according to the plots shown In Figs. 13 and 14, maximum values of bending moment and shear force observed across the wall were 154 kN.m/m and 117 kN/m, respectively, making up M/M_n and V/V_n ratios of 0.07 and 0.12, respectively. A comparison between the obtained values and critical ratios shows that the current conventional design method for diaphragm wall according to the ACI 318 provides a large safety margin and serves as a very suitable approach for the design of a diaphragm wall into an excavation of 10 m in depth.

Figs. 29–31 show variations of M/M_n vs. non-dimensional frequency factor (α). In these figures, the M/M_n value of 0.56 is marked by a column entitled allowable on each plot. Accordingly, the M/M_n values above the allowable value indicate that the safety of diaphragm wall is at risk. Considering the plots demonstrated in Figs. 29–31, it is evident that the value of M/M_n ratio is always larger than allowable limit when the model is subjected to either Tabas or Northridge earthquakes, and always lower than 0.56 when subjected to Whittier Narrows earthquake. It is worth noting that the wall bending which occurred as per numerical analyses under the Tabas and Northridge earthquakes was 2.14 and 2.80 times as large as the corresponding allowable limit, respectively.

Figs. 32–34 show variations of V/V_n vs. non-dimensional frequency factor (α). In these figures marked by a column, the value of 0.47 represents the allowable limit. An increase in the observed shear beyond the allowable limit as per the respective code indicates that the wall is exposed to safety risk. Considering the plots demonstrated in Figs. 32–34, it is evident that the value of V/V_n ratio is always larger than allowable value when the model is subjected to either Tabas or Northridge earthquakes, and always lower than 0.47 when subjected to Whittier Narrows earthquake. As it is evident in the figures, the maximum shear observed as per numerical analyses in the wall under the Tabas and Northridge earthquakes was 2.25 and 2.68 times as large as the corresponding allowable limit, respectively.

4.3. The seismic behavior and design of struts

Evaluated in this section is the behavior and design of lateral bracing for an excavation of 10 m in depth. The behavior of strut during the course of dynamic analysis was evaluated and the maximum value obtained from the analysis was considered as seismic axial strut force. As an example, Fig. 35 presents the history of variations of strut axial force for one of the dynamic analyses. This strut was mounted into a depth of 2 m from the ground level, and the figure shows its behavior in loose soil under Tabas earthquake upon performing the analysis with a bedrock of 60 m in depth. As can be observed in the figure, the maximum axial force in the horizontal brace was recorded at the 15,210th

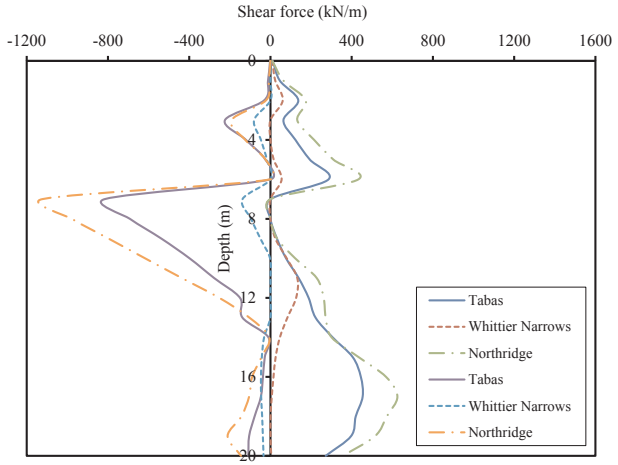

Fig. 28. The comparison of shear wall behavior under various earthquakes.

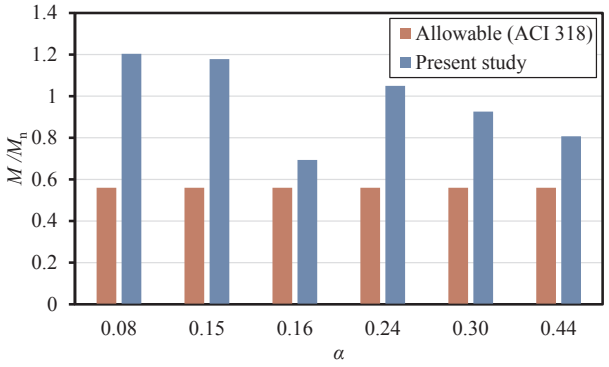

Fig. 29. Assessment of the flexural seismic wall design under Tabas earthquake.

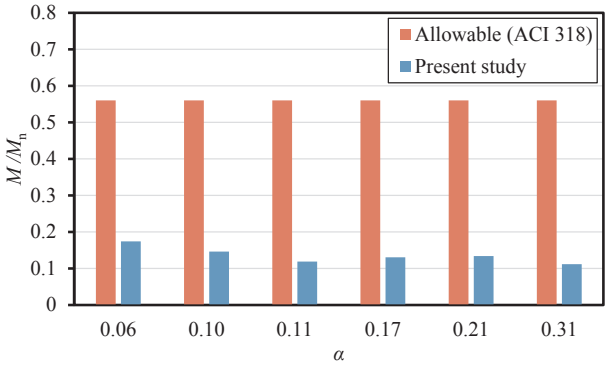

Fig. 30. Assessment of the flexural seismic wall design under Whittier Narrows earthquake.

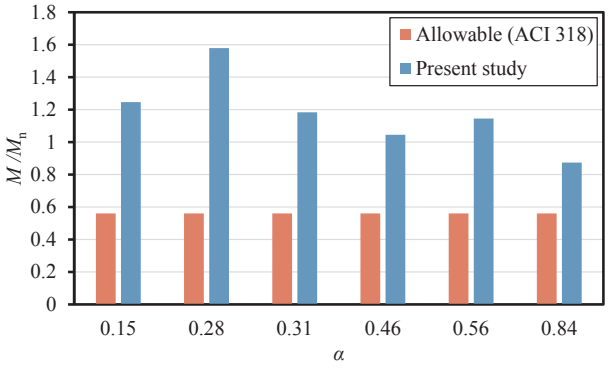

Fig. 31. Assessment of the flexural seismic wall design under Northridge earthquake.

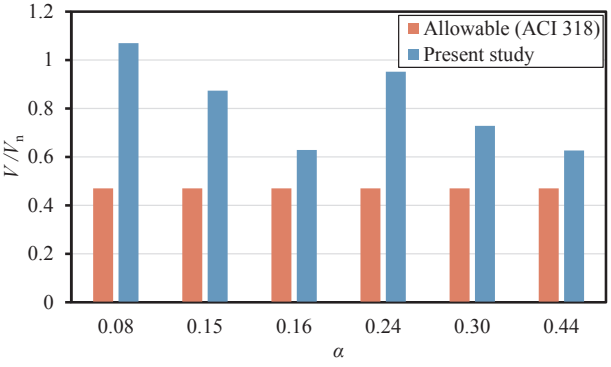

Fig. 32. Assessment of the shear seismic wall design under Tabas earthquake.

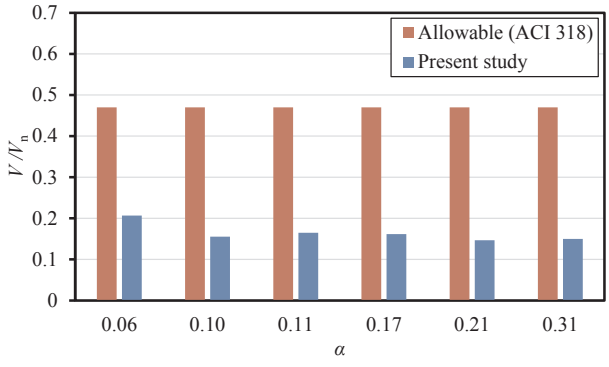

Fig. 33. Assessment of the shear seismic wall design under Whittier Narrows earthquake.

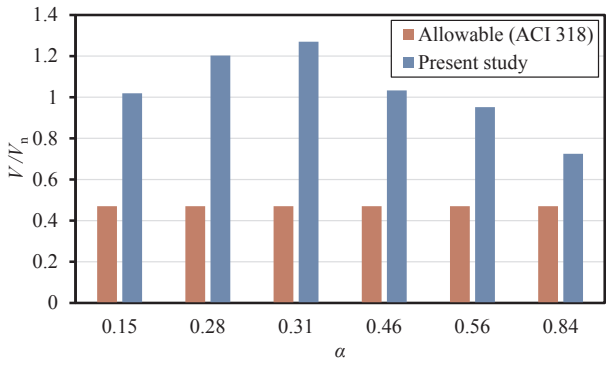

Fig. 34. Assessment of the shear seismic wall design under Northridge earthquake.

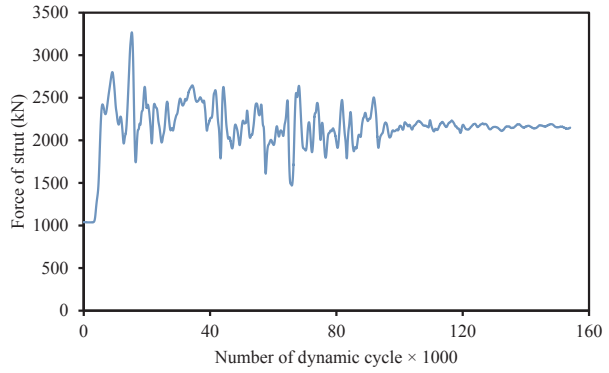

Fig. 35. Variations of axial strut force in the course of seismic loading.

dynamic step. Considering the diagram presented in Fig. 35, it is evident that at the beginning of the dynamic analysis (i.e. static axial force), the strut force is equal to 1037 kN. Moreover, upon termination of applying the Tabas earthquake record to the bedrock at say 124,000th step, fluctuations of the axial strut force were observed to be attenuated.

Axial force and stress of struts at different levels of excavation under static and seismic conditions are compared in Table 6. In this table, F_{st} and F_{se} represent the force of the strut in last excavation step (static condition) and the maximum force existing in the strut during earthquake (seismic condition), respectively. f_a is the maximum existing stress under seismic loading and F_a is the allowable stress, according to AISC [34]. Increasing the ratio of f_a/F_a to values greater than one may put the lateral steel strut at risk of failure, and thus challenge the safety of the excavation.

As seen from Table 6, axial force in the struts under Whittier

Table 6
Comparison of the struts axial stress.

Earthquake name	Depth of bedrock (*m*)	Soil type	Depth of strut (*m*)	F_{st} (*kN*)	F_{se} (*kN*)	$\frac{F_{se}}{F_{st}}$	f_a (*MPa*)	F_a (*MPa*)	$\frac{f_a}{F_a}$	Safety
Tabas	30	LS	2	934	2994	3.21	224.61	131.00	1.71	N.G.
			6	1112	11,135	10.01	835.33	131.00	6.38	N.G.
		DS	2	864	4853	5.62	364.07	131.00	2.78	N.G.
			6	920	16,026	17.42	1202.25	131.00	9.18	N.G.
	60	LS	2	1037	3268	3.15	245.16	131.00	1.87	N.G.
			6	1190	10,919	9.18	819.13	131.00	6.25	N.G.
		DS	2	848	4537	5.35	340.36	131.00	2.60	N.G.
			6	962	10,493	10.91	787.17	131.00	6.01	N.G.
	90	LS	2	1037	3919	3.78	294.00	131.00	2.24	N.G.
			6	1190	9787	8.22	734.21	131.00	5.60	N.G.
		DS	2	848	3912	4.61	293.47	131.00	2.24	N.G.
			6	962	16,054	16.69	1204.35	131.00	9.19	N.G.
Whittier narrows	30	LS	2	934	1584	1.70	118.83	131.00	0.91	O.K.
			6	1112	1981	1.78	148.61	131.00	1.13	N.G.
		DS	2	864	2558	2.96	191.90	131.00	1.46	N.G.
			6	920	2725	2.96	204.43	131.00	1.56	N.G.
	60	LS	2	1037	1381	1.33	103.60	131.00	0.79	O.K.
			6	1190	1496	1.26	112.23	131.00	0.86	O.K.
		DS	2	848	1922	2.27	144.19	131.00	1.10	N.G.
			6	962	1846	1.92	138.48	131.00	1.06	N.G.
	90	LS	2	1037	1603	1.55	120.26	131.00	0.92	O.K.
			6	1190	1385	1.16	103.90	131.00	0.79	O.K.
		DS	2	848	2413	2.85	181.02	131.00	1.38	N.G.
			6	962	2112	2.20	158.44	131.00	1.21	N.G.
Northridge	30	LS	2	934	3144	3.37	235.86	131.00	1.80	N.G.
			6	1112	14,910	13.41	1118.53	131.00	8.54	N.G.
		DS	2	864	4039	4.67	303.00	131.00	2.31	N.G.
			6	920	15,900	17.28	1192.80	131.00	9.11	N.G.
	60	LS	2	1037	3949	3.81	296.25	131.00	2.26	N.G.
			6	1190	14,644	12.31	1098.57	131.00	8.39	N.G.
		DS	2	848	4770	5.63	357.84	131.00	2.73	N.G.
			6	962	19,277	20.04	1446.14	131.00	11.04	N.G.
	90	LS	2	1037	3658	3.53	274.42	131.00	2.09	N.G.
			6	1190	11,135	9.36	835.33	131.00	6.38	N.G.
		DS	2	848	4785	5.64	358.96	131.00	2.74	N.G.
			6	962	14,462	15.03	1084.92	131.00	8.28	N.G.

Narrows earthquake is almost three times larger in the static condition, whereas, it presents much larger amounts in the case of Tabas and Northridge earthquakes. The F_{se}/F_{st} increases to 17 and 20 in the Tabas and Northridge earthquakes, respectively, which implies that the seismic force of struts is much larger than static force and the safety of lateral supports is severely threatened. Since the f_a/F_a increases to one in all struts during the Tabas and Northridge earthquakes, then they are under threat of failure. Struts under the Whittier Narrows earthquake are relatively safe in loose sand, but in dense sand, all of the struts are in danger of failure.

The results of the present section revealed that the traditional method of lateral bracing design is not efficient in dealing with seismic loads. Especially with increasing soil stiffness or the occurrence of long-lasting earthquakes, struts safety is severely compromised.

5. Conclusions

In this study, seismic behavior of diaphragm wall in sandy soil for a 10 m excavation has been assessed. The analyses were accomplished in two sandy soils with shear modulus of 53 and 180 MPa. The range of shear modulus of sand is wide enough to generalize the present results to other braced excavations in sand. Three Tabas, Whittier Narrows and Northridge earthquakes with different PGAs and frequency contents have been applied to bedrocks with depth of 30, 60 and 90 m. Two rows of struts were used over the wall to prevent wall horizontal displacement at depths of 2 and 6 m. It is worth noting that a total of 18 cases were analyzed in this paper. The range of PGA is in between 0.32 and 0.73 g and the range of significant duration is in between 1.22 and 11.32 s. The range of PGA and significant durations are high and wide enough to cover most of the known earthquakes. Thus, the behavioral pattern acquired in this paper can be reliable for other earthquakes. Diaphragm wall was designed based on the requirements of ACI 318. Additionally, struts were designed using Peck method and were controlled by AISC regulation. By comparing the results of the numerical analysis and the allowable limits in the regulation assessment, the limitations of the common methods of excavation components design were evaluated. The results of the numerical research are as follows:

A. According to the evaluations of the present paper, it was concluded that the reciprocal support method is an acceptable method in static condition but not a desirable method to control displacement of the walls under seismic loads, especially in the sites with dense sand.
B. Comparison of the results of the present numerical analysis with ACI 318 design method reveals that the diaphragm walls designed by ACI 318 under static loads have enough safety and hence absolutely suitable for designing an excavation. However, based on the results of the numerical analysis, bending moment and shear force of the diaphragm walls under seismic loads were observed to reach 2.8 and 2.7 times as large as the respective allowable limits. Therefore, cautions should be taken in seismic design of diaphragm walls using ACI 318 code requirements.
C. Assessments which have been done in this study indicated that Peck method is completely capable to design the lateral brace for a 10 m excavation for various kinds of sandy soils and the lateral bracing is an efficient method for providing the excavation safety under static loads but steel struts do not show a good performance under dynamic loads and the axial stresses were observed up to 11 times higher than the allowable stress and therefore the safety aspects

should be thoroughly considered to provide the excavation safety in earthquake-prone areas and under dynamic loads.

D. Two opposite walls in braced excavation may cause different seismic behaviors. This paper evaluations showed that the behavior of left and right walls in the braced excavation with a width of 10 m in sandy soils is not much different.

E. The study showed that earthquakes that had higher significant duration, and exerted their energy into site during more times would show higher destructive effects. Therefore the significant duration of earthquake is a very important factor in designing underground walls.

References

[1] Ou CY, Chiou DC, Wu TS. Three-dimensional finite element analysis of deep excavations. J Geotech Eng 1996;122(5):337–45.
[2] Bose S, Som N. Parametric study of a braced cut by finite element method. Comput Geotech 1998;22(2):91–107.
[3] Faheem H, Cai F, Ugai K. Three-dimensional base stability of rectangular excavations in soft soils using FEM. Comput Geotech 2004;31(2):67–74.
[4] Zdravkovic L, Potts DM, John HDS. Modelling of a 3D excavation in finite element analysis. Géotechnique 2005;55(7):497–513.
[5] Finno RJ, Blackburn JT, Roboski JF. Three-dimensional effects for supported excavations in clay. J Geotech Geoenviron Eng 2007;133(1):30–6.
[6] Arai Y, Kusakabe O, Murata O, Konishi S. A numerical study on ground displacement and stress during and after the installation of deep circular diaphragm walls and soil excavation. Comput Geotech 2008;35(5):791–807.
[7] Yoo C, Lee D. Deep excavation-induced ground surface movement characteristics – a numerical investigation. Comput Geotech 2008;35(2):231–52.
[8] Hsiung B-CB. A case study on the behaviour of a deep excavation in sand. Comput Geotech 2009;36(4):665–75.
[9] Ou CY, Hsieh PG. A simplified method for predicting ground settlement profiles induced by excavation in soft clay. Comput Geotech 2011;38(8):987–97.
[10] Chowdhury SS, Deb K, Sengupta A. Estimation of design parameters for braced excavation: numerical study. Int J Geomech 2013;13(3):234–47.
[11] Ou CY, Hsieh PG, Lin YL. A parametric study of wall deflections in deep excavations with the installation of cross walls. Comput Geotech 2013;50:55–65.
[12] Bahrami M, Khodakarami MI, Haddad A. 3D numerical investigation of the effect of wall penetration depth on excavations behavior in sand. Comput Geotech 2018;98(1):82–92.
[13] Hsieh PG, Ou CY. Shape of ground surface settlement profiles caused by excavation. Can Geotech J 1998;35(6):1004–17.
[14] Long M. Database for retaining wall and ground movements due to deep excavations. J Geotech Geoenviron Eng 2001;127(3):203–24.
[15] Moormann C. Analysis of wall and ground movements due to deep excavations in soft soil based on a new worldwide database. Soils Found 2004;44(1):87–98.
[16] Liu G, Ng CW, Wang Z. Observed performance of a deep multistrutted excavation in Shanghai soft clays. J Geotech Geoenviron Eng 2005;131(8):1004–13.
[17] Kung GT, Juang CH, Hsiao EC, Hashash YM. Simplified model for wall deflection and ground-surface settlement caused by braced excavation in clays. J Geotech Geoenviron Eng 2007;133(6):731–47.
[18] Wang J, Xu Z, Wang W. Wall and ground movements due to deep excavations in Shanghai soft soils. J Geotech Geoenviron Eng 2010;136(7):985–94.
[19] Bahrami M, Khodakarami MI, Haddad A. Assessment of the effect of pre-stressing steel strut on displacement of the diaphragm wall and the soil. J Civil Environ Eng 2017.
[20] Madabhushi S, Zeng X. Seismic response of gravity quay walls II: numerical modeling. J Geotech Geoenviron Eng 1998;124(5):418–27.
[21] Caltabiano S, Cascone E, Maugeri M. Seismic stability of retaining walls with surcharge. Soil Dyn Earthquake Eng 2000;20(5):469–76.
[22] Gazetas G, Psarropoulos P, Anastasopoulos I, Gerolymos N. Seismic behaviour of flexible retaining systems subjected to short-duration moderately strong excitation. Soil Dyn Earthquake Eng 2004;24(7):537–50.
[23] Psarropoulos P, Klonaris G, Gazetas G. Seismic earth pressures on rigid and flexible retaining walls. Soil Dyn Earthquake Eng 2005;25(7):795–809.
[24] Wartman J, Rondinel-Oviedo EA, Rodriguez-Marek A. Performance and analyses of mechanically stabilized earth walls in the Tecoman, Mexico earthquake. J Perform Constr Facil 2006;20(3):287–99.
[25] Callisto L, Soccodato F. Seismic design of flexible cantilevered retaining walls. J Geotech Geoenviron Eng 2010;136(2):344–54.
[26] Chowdhury SS, Deb K, Sengupta A. Behavior of underground strutted retaining structure under seismic condition. Earthquakes Struct 2015;8(5):1147–70.
[27] Konai S, Sengupta A, Deb K. Behavior of braced excavation in sand under a seismic condition: experimental and numerical studies. Earthquake Eng Eng Vibrat 2018;17(2):311–24.
[28] Itasca. Fast Lagrangian analysis of continua. Minneapolis (Minn): Itasca Consulting Group Inc; 2016.
[29] Ohsaki Y, Iwasaki R. On dynamic shear moduli and Poisson's ratios of soil deposits. Soils Found 1973;13(4):61–73.
[30] Janbu N. Soil compressibility as determined by odometer and triaxial tests. Eur Conf Soil Mech Found Eng Wiesbaden 1963:19–25.
[31] Jaky J. The coefficient of earth pressure at rest. J Soc Hungarian Arch Eng 1944;78(22):355–8.
[32] Aversa S, Maiorano R, Tamagnini C. Influence of damping and soil model on the computed seismic response of flexible retaining structures. 14th European Conference on Soil Mechanics and Geotechnical Engineering. 2007.
[33] ACI. 318-14. Building code requirements for structural concrete. Farmington Hills (Michigan): American Concrete Institute; 2014.
[34] AISC L. Design RF. Manual of steel construction. American Institute of Steel Construction; 2001.
[35] Peck RB. Deep excavation and tunneling in soft ground. 7th international conference on soil mechanics and foundation engineering. Mexico City, Mexico. 1969. p. 225–90.
[36] Lysmer J, Kuhlemeyer R. Finite element model for infinite media. J Eng Mech Div 1969;95:859–77.
[37] Trifunac MD, Brady AG. A study on the duration of strong earthquake ground motion. Bull Seismol Soc Am 1975;65(3):581–626.
[38] Kramer SL. Geotechnical earthquake engineering. New York: Prentice Hall; 1996.